Materials Research Proceedings 28 (2023) 1379-1386 https://doi.org/10.21741/9781644902479-149

Simple multiaxial tests to assess dynamic ductility of 17-4PH

MANCINI Edoardo[1,a *], CORTIS Gabriele[2,b], CORTESE Luca[2,c], UTZERI Mattia[3,d] and SASSO Marco[3,e]

[1] Università degli Studi dell'Aquila, DIIIE, Piazzale Ernesto Pontieri I, 67100 L'Aquila, Italy

[2] Sapienza University of Rome, Via Eudossiana 18, 00184 Rome, Italy

[3] Università Politecnica delle Marche, DIISM, Via Brecce Bianche, 60121 Ancona, Italy

[a]edoardo.mancini@univaq.it, [b]gabriele.cortis@uniroma1.it, [c]luca.cortese@uniroma1.it, [d]m.utzeri@pm.univpm.it, [e]m.sasso@staff.univpm.it

Keywords: Ductile Damage Modelling, High Strain Rate, Material Characterization

Abstract. To investigate material ductility, the use of simple multiaxial specimens which can be tested through a common tensile machine or by a Split Hopkinson bar facility would allow avoiding the use of more complex equipment to induce different stress states in the investigated material. In this work, experimental dynamic tests have been performed on four different specimen geometries on a 17-4PH steel by a direct Split Hopkinson Bar (SHB). Finite element models of the experiments are set up and used jointly with experimental data to calibrate and validate a strain rate dependent plasticity model, and to extract the local values of stress and ultimate strain in the most critical point of the samples, at fracture. These latter results allowed the calibration of a ductile damage model, whose predictions, compared with a previous calibration using tests carried out in quasi-static conditions, confirmed the effectiveness of the proposed specimens and test methodology to assess material ductility under dynamic conditions.

Introduction

To provide an accurate evaluation of material plastic strain at failure which is crucial in different fields of mechanical design, different ductile damage models have been developed in the literature to describe how a material gets damaged with plastic deformation until reaching its ultimate strength. They can be classified according to their driving principle: starting from those thermodynamically based [1,2], through criteria relying on the evolution of micro-void [3] up to empirical-based formulations [4]. All of them require different experimental tests for their calibration (such as tensile tests on round smooth or notched bar, torsion or compression tests and often multi-axial tests) and often special testing set-ups, involving a complex experimental phase and tuning procedures, which are non-trivial and not suitable for companies which sometimes may not have specific facilities available. These difficulties are greater under dynamic conditions due to the special devices required for multiaxial tests execution, as to achieve combined tension-torsion [5].

The aim of this paper is to validate, under dynamic conditions, the effectiveness of simple specimen geometries capable of inducing different multi-axial stress states in the material, to be tested using a conventional SHB, in order to simplify the experimental phase of material characterization. Starting from the geometry proposed by Driemeier et al. [6] and improved by Cortis et al. [7], different simulations have been carried out to identify the most suitable sample proportions and dimensions for dynamic tests. In order to reproduce additional loading conditions, round bar (RB) and round notched bar (RNB) specimens have been tested too. Using the results obtained from the dynamic tests made on these new simple specimens, a ductile damage model

Materials Research Proceedings 28 (2023) 1379-1386 https://doi.org/10.21741/9781644902479-149

has been calibrated, and its prediction was compared with that one obtained from a previous calibration obtained by testing the same sample geometries under quasi-static conditions.

Material and Methods

Plasticity Model. Among the constitutive models available in the literature, suitable to describe the flow stress in a material as a function of strain, strain rate and temperature, the Johnson and Cook (JC) [8] was considered. The model is based on Mises Plasticity and accounts for strain hardening, strain rate and thermal softening:

$$\sigma = (A + B\varepsilon^n)\left[1 + C\ln\left(\frac{\dot{\varepsilon}}{\dot{\varepsilon}_0}\right)\right]\left[1 + \left(\frac{T - T_0}{T_{melt} - T_0}\right)^m\right] \quad (1)$$

In Eq. 1 ε, $\dot{\varepsilon}$, $\dot{\varepsilon}_0$, T_0 and T_{melt} are the equivalent plastic strain, the plastic strain rate, the reference strain rate, the room temperature and the melting temperature of the material while *A, B, n, C* and *m* are the constants to be calibrated.

Damage model. Ductile damage models belonging to the class of empirical formulations are represented by a scalar *D* that increases proportionally with the equivalent plastic strain ε_p weighted on a function of the stress state $f(T, X)$;

$$D = \int_0^{\varepsilon_f} f(T, X) d\varepsilon_p \quad (2)$$

where the triaxiality *T* and the Lode parameter *X* are the two scalars describing the stress state (Eq. 3).

$$T = \frac{1}{3}\frac{I_1}{\sqrt{3J_2}}; X = \frac{27}{2}\frac{J_3}{\left(\sqrt{3j_2}\right)^3} \quad (3)$$

Where I_1 is the first stress invariant, J_2 and J_3 are the second and the third deviatoric stress invariants, respectively. Material failure occurs when *D* reaches a critical value set equal to 1.

Under proportional loading conditions, which implies *T* and *X* constant with plastic strain, it is possible to invert Eq. 2 to obtain the following expression:

$$\varepsilon_f = f^{-1}(T, X) \quad (4)$$

which represents a "Fracture Surface" in the space (T, X, ε_f). $f^{-1}(T, X)$ can be described by different expressions; in the present work, the Coppola-Cortese (CC) [9] formulation was adopted:

$$\varepsilon_f = \frac{1}{A_1} e^{-A_2 T}\left(\frac{cos\left[\beta\frac{\pi}{6} - \frac{1}{3}arccos(\gamma)\right]}{cos\left[\beta\frac{\pi}{6} - \frac{1}{3}arccos(\gamma X)\right]}\right)^{\frac{1}{n}} \quad (5)$$

Materials Research Proceedings 28 (2023) 1379-1386 https://doi.org/10.21741/9781644902479-149

where A_1, A_2, β and γ are material constants that define the surface shape, while n represents the strain hardening exponent of a Hollomon's power law fit of the stress-strain curve: $\sigma = K\varepsilon^n$.

Materials. All specimens were manufactured from a single wrought bar. The investigated material is a 17-4PH steel that was characterised already under static conditions by some of the authors [7]. In order to compare the fracture surface obtained at a high strain rate with that one in static conditions, the calibration will be performed using multiaxial tests similar to those used in the static investigation, namely the improved "Driemeier" specimens and the RB and RNB specimens. In this work, two different configurations of the central holes of the Driemeier geometry were selected, corresponding to two different angles (α) of 10° and 30°, hereafter referred to as Pos10 and Pos30, respectively. The two angles were chosen to generate proper combinations of tensile-shear stress states. Moreover, to obtain similar strain rates from all tests, an optimization procedure was used to identify the sample dimensions, as reported in the next sub-section, "Samples for Dynamic Tests".

The final specimen dimensions are shown in Fig. 1. They were machined from metal bars with a diameter of 20 mm. The thickness of the gauge region of samples (a) and (b) is constant and equal to 2 mm.

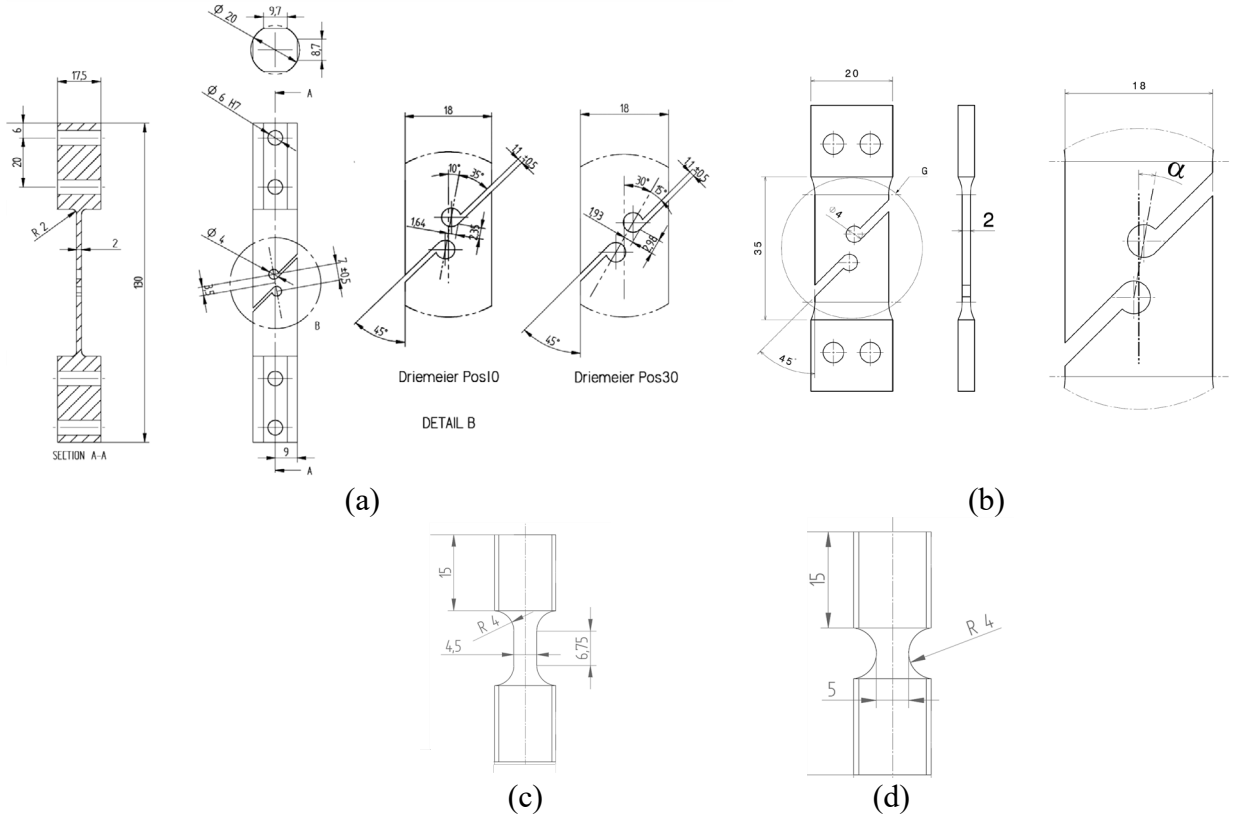

Fig. 1. Optimised geometries: Driemeier Pos10 and Pos30 for quasi-static (a) and dynamic tests (b); RB (c) and RNB (d) for dynamic tests.

Equipment. Quasi-static tests were performed in [7] by a universal servo-hydraulic MTS with 250 kN maximum load. Instead, a custom direct split Hopkinson bar [10] was used for dynamic tests. It consists of three aligned bars, named the pre-stressed, input and output bars. A tensile input wave (σ_i) is generated by pre-loading the pre-stressed bar in compression; the subsequent sudden release of this pre-load generates the waves that deform dynamically the sample (Fig. 2). By acquiring the transmitted and reflected waves (σ_t, σ_r) using properly placed strain gages and assuming uniaxial wave propagation in the bars and dynamic equilibrium in the sample, the dynamic properties, as well as the displacements u at the lateral faces of the specimen, can be assessed [10]. Moreover, digital images of all tests have been acquired using a FastCam at 100 kfps.

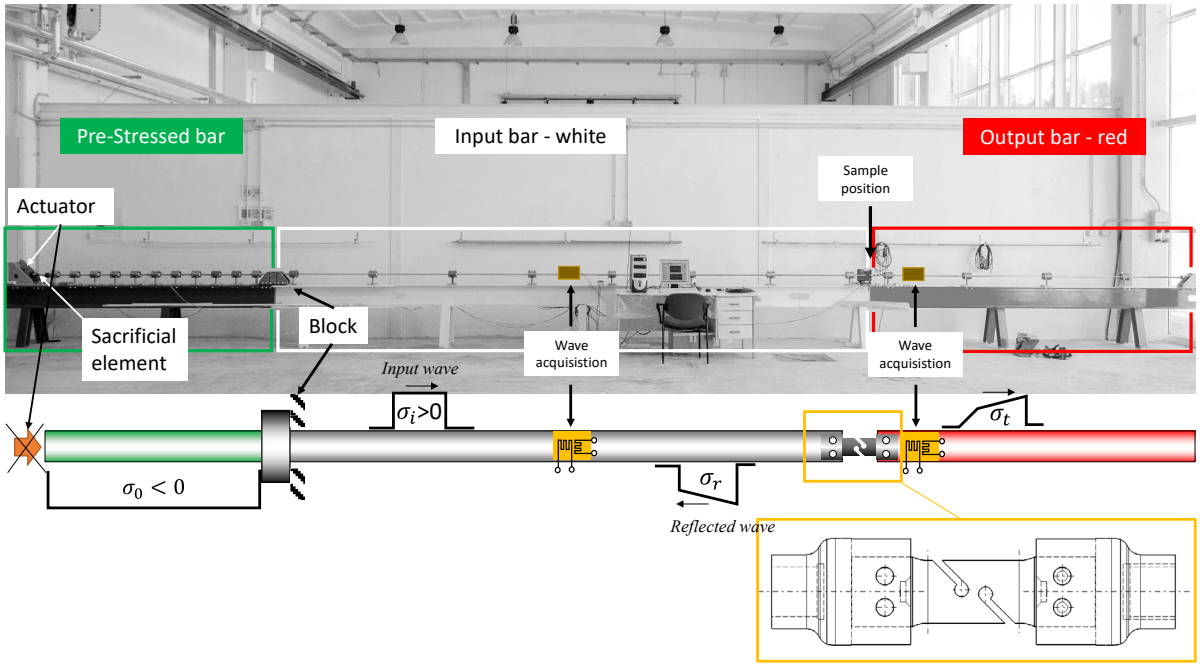

Fig. 2. Direct Split Hopkinson bar, and details the improved Driemeier sample and fasteners.

Samples for Dynamic Tests. The geometries of the samples used in the dynamic tests essentially consist of modifications of those used in the quasi-static tests, to adapt them to the available SHB equipment. Basically, the dynamic tests specimens must meet the geometric requirements in length and cross-section, to be mounted and successfully tested on the Hopkinson bar; in addition, the same equivalent plastic strain rate should be achieved in all tests. To meet these requirements, an inverse Finite Element (FE) approach was implemented according to a previously developed procedure [11,12], where the tests on RB, RNB and Driemeier samples are reproduced by FE simulations. The shape and size of the Driemeier specimens were maintained, whereas the cross-section diameter and the fillet of the RB and RNB specimens were iteratively varied according to a full factorial Design of Experiment plan; moreover, the impact intensity, i.e. the boundary velocity, was varied as well. Eventually, a combination of parameters has been found that permits the achievement of similar average plastic strain rates in the four different tests.

Of course, this is an approximate method, in which reasonable values for the material stress-strain curve as well as for the material strain to failure are assumed, not being known a priori.

The final dimensions adopted in the tests for RB and RNB samples are reported in Fig. 1.

Materials Research Proceedings 28 (2023) 1379-1386 https://doi.org/10.21741/9781644902479-149

Results and Discussion

The experimental results were first used to calibrate the JC constitutive material model. The material constants were derived through an inverse procedure by means of Finite Element simulations of the tests, minimizing the difference between experimental and numerical load-displacement global data. The comparison of the experimental curves with those obtained by the FE simulations using best fit JC material constants are shown in Fig. 3, where the red dots represent the onset of failure. Three repetitions were performed for each text and the experimental curves in the graphs represent the average data.

Concerning the RB and RNB tests an excellent numerical-experimental match is observed, even for Driemeier Pos10 and Pos30, although small discrepancies are shown, the match is fairly good. In Fig. 4 the distribution of equivalent plastic strain is reported, which fulfils one of the design requirements, namely the concentration of the maximum plastic strain value at its critical point in the centre of the gauge.

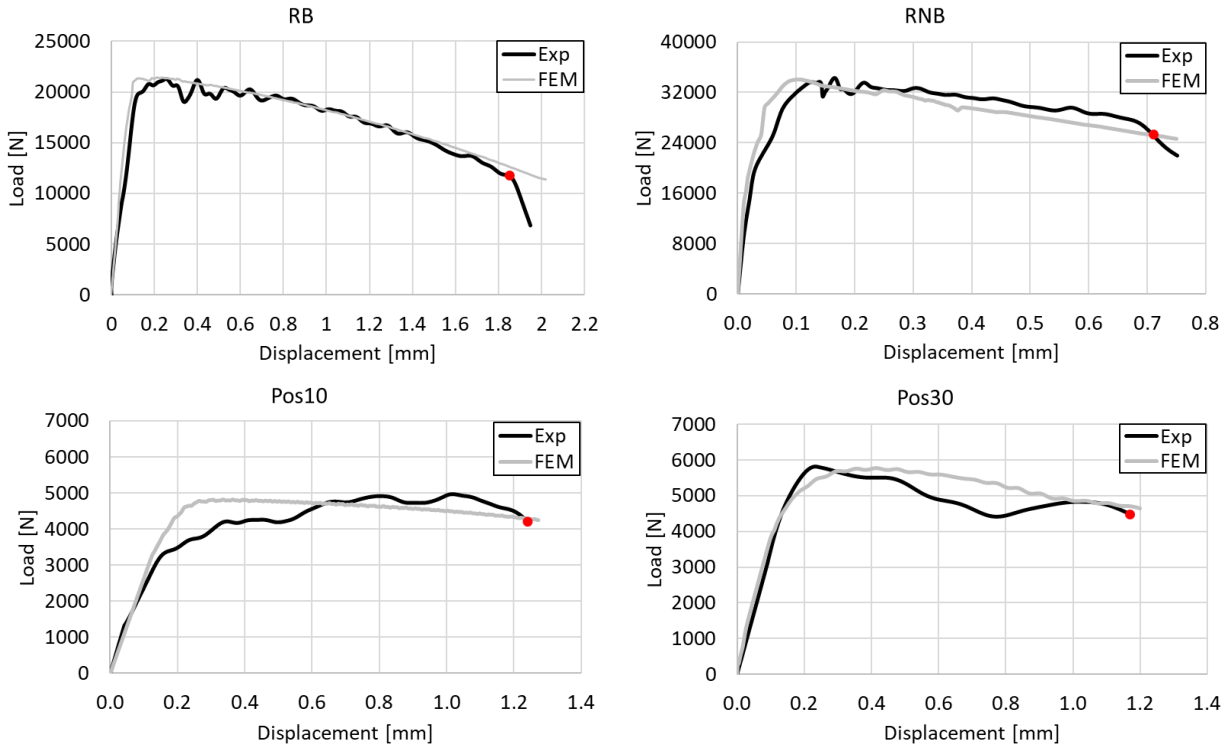

Fig. 3. Comparison between experimental and numerical load-displacement curves for RB, RNB, Pos10 and Pos30 tests. The red dots represent the onset of failure.

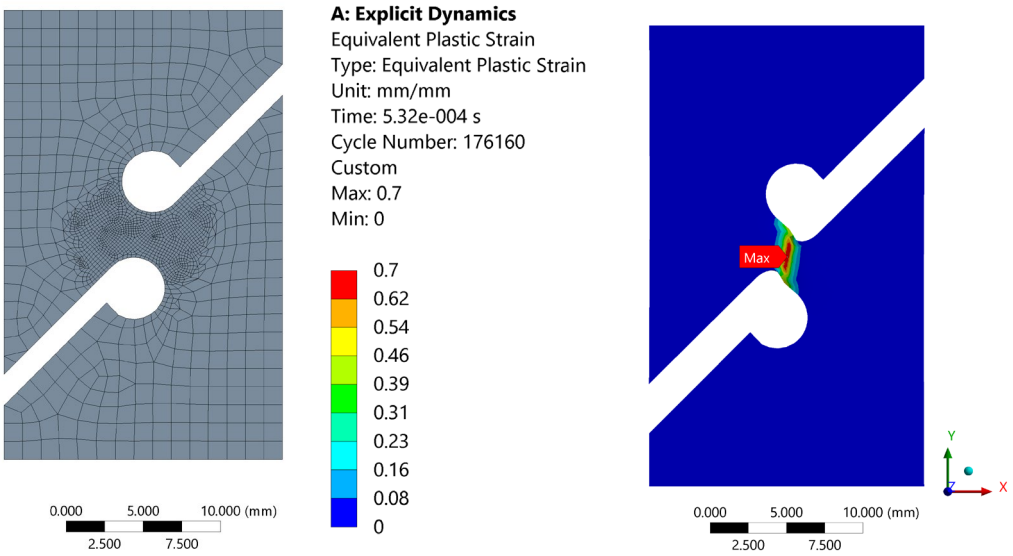

Fig. 4. Driemeier Pos 10°, mesh detail and contour plot of equivalent plastic strain.

After validating the FEM models by means of the numerical-experimental comparison presented above, the parameters T, X and ε_p were derived, for each test, at the critical point and at the instant of failure. These data are reported in Table 1, for both static and dynamic conditions. Subsequently, the CC damage model was calibrated through a minimisation algorithm, namely the calibration constants (A_1, A_2, β, γ) were derived such that the resulting fracture surface was as close as possible to the T, X and ε_p experimental points.

Table 1. Values of $\boldsymbol{T}$, $\boldsymbol{X}$ *and* $\boldsymbol{\varepsilon_p}$ *for static and dynamic tests.*

	Static			Dynamic		
	T	X	ε_p	T	X	ε_p
Pos10	0.05	0.16	0.33	0.13	0.41	0.70
Pos30	0.10	0.38	0.46	0.26	0.71	0.83
RB	0.61	0.99	1.17	0.67	0.99	0.78
RNB	0.76	0.99	0.81	1.07	0.99	0.40

Fig. 5a illustrates the dynamic and static fracture surfaces predicted by CC damage model, using the JC as plasticity model. In addition, a two dimensional view of ε_p as a function of the T along curves at constant X has been reported (Fig. 5b).

The dynamic fracture surface showed a good match with the experimental points (Fig. 5b). It is worth noting that the static-dynamic comparison suggests an increase in the ductility of the 17-4PH as the strain rate is increased, overall. More in detail, the dynamic fracture surfaces were slightly below the static fracture surfaces at high triaxialities (T around 1), remaining higher for medium and low triaxialities.

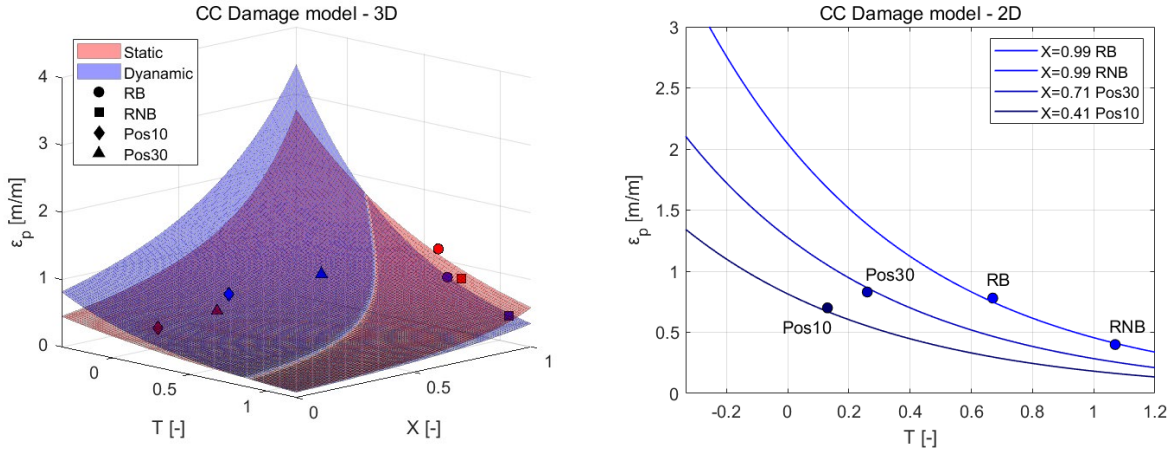

(a) (b)

Fig. 5. 3D (a) and 2D (b) views of 17-4PH fracture surfaces obtained under quasi-static and dynamic conditions, with indications of the strain to fracture of the RB, RNB, Pos10 and Pos30 tests.

Summary

In this work, the possibility of adopting simple multiaxial specimens for material characterization tests at high strain rates was investigated. The ductility of a 17-4PH steel alloy at high strain rates, as estimated by a damage model proposed by one of the authors, was evaluated and compared with the corresponding material behaviour under static conditions. Tensile specimens, such as round bars and round notched bars, together with the simple multiaxial specimens, were used. The dynamic experimental campaign was carried out by a direct split Hopkinson bar. The results highlighted the differences in terms of static-dynamic ductility of 17-4PH, and showed the suitability of the proposed approach to calibrate a ductile damage model at a high strain rate, using a standard dynamic testing equipment.

References

[1] J. Lemaitre, A continuous damage mechanics model for ductile fracture, J. Eng. Mater. Technol. 107 (1985) 83-89.

[2] N. Bonora, A nonlinear CDM model for ductile failure, Eng. Fract. Mech. 58 (1997) 11-28.

[3] J.W. Hancock, A.C. Mackenzie, On the mechanism of ductile failure in high-strength steel subjected to multi-axial stresses, J. Mech. Phys. Solids 24 (1976) 147-169.

[4] D.M. Jr Norris, J.E. Reaugh, B. Moran, D. F. Quinnones, A plastic-strain mean-stress criterion for ductile fracture, J. Eng. Mater. Technol. 100 (1978) 279-286.

[5] M. Sasso, E. Mancini, Feasibility Study of a Combined Tension-Torsion Hopkinson Bar, EPJ Web Conf. Volume 250, 2021, DYMAT 2021 - 13th Int. Conference on the Mechanical and Physical Behaviour of Materials under Dynamic Loading

[6] L. Driemeier, M. Brünig, G. Micheli, M. Alves, Experiments on stress-triaxiality dependence of material behavior of aluminum alloys, Mech. Mater. 42 (2010) 207-217. https://doi.org/10.1016/j.mechmat.2009.11.012

[7] G. Cortis, F. Nalli, M. Piacenti, A direct methodology for the calibration of ductile damage models from a simple multiaxial test, IOP Conf. Ser. (2021), Mater. Sci. Eng. 1214 (2021) 012016. https://doi.org/10.1088/1757-899X/1214/1/012016

[8] G.R. Johnson, W.H. Cook, A constitutive model and data for metals subjected to large strains, high strain rates, and high temperatures, Proceedings of the Seventh International Symposium on Ballistics, International Ballistics Committee, Hague, The Netherlands, 19-21 (1983) 541-547.

[9] T. Coppola, L. Cortese, P. Folgarait, The effect of stress invariants on ductile fracture limit in steels, Eng. Fract. Mech. 76 (2009) 1288-1302. https://doi.org/10.1016/j.engfracmech.2009.02.006
[10] E. Mancini; M. Sasso, M. Rossi, G. Chiappini, G. Newaz, D. Amodio, Design of an Innovative System for Wave Generation in Direct Tension-Compression Split Hopkinson Bar, J. Dyn. Behav. Mater.1 (2015) 201-213. https://doi.org/10.1007/s40870-015-0019-1
[11] M. Sasso, E. Mancini, L. Cortese, F. Nalli, Design and Optimization of Dynamic Test Samples for Ductile Damage Assessment, In Proceedings of the DYMAT 2018 - 12th International Conference on the Mechanical and Physical Behaviour of Materials under Dynamic Loading, Arcachon, France, 9-14 September 2018. https://doi.org/10.1051/epjconf/201818301061
[12] G. Cortis, F. Nalli, M. Sasso, M. L. Cortese, E. Mancini, Effects of Temperature and Strain Rate on the Ductility of an API X65 Grade Steel, Appl. Sci. 12 (2022) 2444. https://doi.org/10.3390/app12052444